Collisional shifts in one- and two-dimensional shallow blue-detuned ^{87}Sr optical lattice clocks

Deshui Yu*

Department of Applied Physics, Graduate School of Engineering, The University of Tokyo, Bunkyo-ku, Tokyo 113-8656, Japan

(Received 22 January 2012; published 12 March 2012)

We study the influence of ultracold collisions induced by the inhomogeneous excitation on the clock-transition frequency in one- and two-dimensional shallow blue-detuned (BD) ^{87}Sr optical lattice clocks with a magic wavelength of $\lambda_b = 389.889$ nm. The minimal lattice potential required to tightly confine atoms in each single lattice site is much larger than that required for a red-detuned (RD) lattice operating at $\lambda_r = 813.4$ nm because of the relatively smaller magic wavelength. For a deep optical lattice, the two-body interactions of atoms in a single lattice site mainly contribute to the clock-transition frequency shift, while the intersite collisions primarily affect the collisional shift in a shallow optical lattice. For an effective misalignment angle $\Delta\theta \sim 10$ mrad of the probe beam with respect to the lattice axis, the fractional collisional shifts in both one- and two-dimensional BD lattices are at the 10^{-16} level.

DOI: 10.1103/PhysRevA.85.032705 PACS number(s): 34.50.Cx, 06.30.Ft, 32.30.−r

I. INTRODUCTION

An optical lattice clock [1–4] with a large number of quantum absorbers separately trapped in the Lamb-Dicke regime and with a zero net ac Stark shift of the clock transition provides an opportunity to realize an exceptionally low instability of 10^{-18} in one second. However, this vast potential has not yet been realized due to thermal-noise-limited laser sources [5–8], the Dick effect resulting from the unavoidable dead time during periodic interrogations [9,10], the collisional frequency shift caused by the excitation inhomogeneity [11–13], and the polarization-dependent and higher-order light shifts [14–17].

Recently, by applying a cavity-stabilized laser system with a reduced thermal noise floor, a measurement consistent with a clock instability of $5 \times 10^{-16}/\sqrt{\tau}$ has been achieved based on a ytterbium optical lattice clock [18]. In addition, a synchronous frequency comparison between a one-dimensional (1D) ^{87}Sr lattice clock and a three-dimensional (3D) ^{88}Sr lattice clock has reached an extremely low Allan standard deviation of 1×10^{-17} approaching the quantum projection noise limit in an averaging time of 10^3 s by cancelling out the Dick effect [19].

The density-dependent collisional frequency shift induced by the inhomogeneity in the probe excitation was first probed in a 1D spin-polarized ^{87}Sr lattice clock [11]. For ^{87}Sr atoms tightly confined in a two-dimensional (2D) lattice, the antisymmetric spin state (singlet) and the symmetric triplet states are well separated [20], for which the small excitation inhomogeneity hardly induces a transition between the singlet and triplet states. As a result, the collisional frequency shift of clock transition is significantly suppressed [21]. Additionally, collisional shift can be dramatically suppressed by confining atoms in a 3D lattice with a filling factor less than or equal to 1 per lattice site [22]. However, the huge vector and tensor light shifts inhibit the realization of a 3D fermionic lattice clock. On the other hand, the scattering losses induced by the inelastic collisions in Sr and Yb optical lattice clocks have been experimentally investigated in Refs. [23–25].

The nonscalar light shifts can be reduced via a blue-detuned (BD) lattice with a trap potential as shallow as possible. For a BD ^{87}Sr lattice clock with a magic wavelength of $\lambda_b = 389.889$ nm [26], atoms are trapped in the intensity minima of the trapping field and are therefore minimally perturbed by the lattice field, which is completely contrary to the case of a red-detuned (RD) lattice operating at a magic wavelength $\lambda_r = 813.4$ nm. In addition, working with dipole traps as shallow as possible is required not only for reducing the multipolar perturbation [27], but also for the technical aspects.

So far, a shallow BD lattice clock has not been studied in depth. In this article, based on ^{87}Sr atoms, we investigate the collisional shifts in both 1D and 2D shallow BD optical lattice clocks, where the influence of intersite collisions on the clock-transition frequency cannot be ignored besides the two-body interactions of atoms at the same lattice site. Due to the relatively smaller magic wavelength comparing with λ_r, atoms cannot be tightly confined in a single BD lattice site with a trap potential similar to that used in the RD lattice estimated in Ref. [28]. We compare influences of the two-body interactions of atoms in a single lattice site and the intersite collisions of atoms in different lattice sites on the density-dependent frequency shift and find that the former interactions mainly contribute to the frequency shift in a deep lattice while the latter collisions primarily affect the collisional shift in a shallow lattice. We also study the dependence of collisional shift on atomic temperature and the area of the probe pulse.

This article is organized as follows: In Sec. II we consider the spin-polarized atoms with s-wave interactions in a 1D shallow BD lattice. Based on the conclusions derived from a simple four-atom system, the many-particle system can be reduced to a solvable spin-$\frac{1}{2}$ model, and the collision-induced frequency shift is studied by applying this simple model in Sec. III. Section IV describes the suppression of collisional shift in a 2D shallow BD lattice. Finally, we summarize our discussion in Sec. V.

II. SPIN-POLARIZED ATOMS IN 1D OPTICAL LATTICE

A. Physical model

We consider an ensemble of spin polarized fermionic ^{87}Sr ($I = 9/2$) trapped in a 1D BD optical lattice with a magic

*dsyu@amo.t.u-tokyo.ac.jp

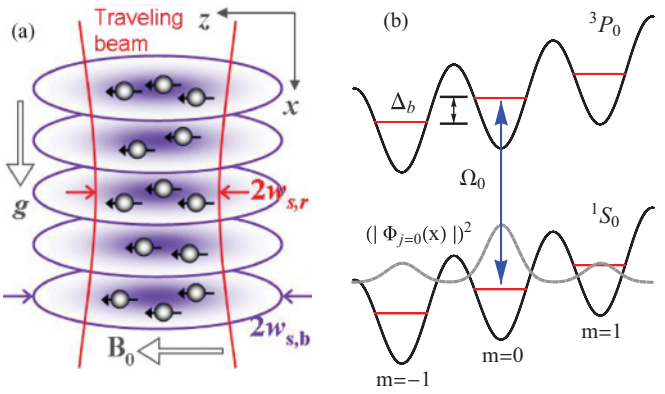

FIG. 1. (Color online) Scheme of 1D BD optical lattice clock. (a) A BD lattice is formed by a linearly polarized standing wave operating at λ_b in the vertical x direction. A RD linearly polarized traveling beam overlaps the BD lattice in the same direction, and its beam waist $w_{s,r}$ is much smaller than that of the lattice beam $w_{s,b}$, while its intensity is large enough that atoms can be weakly confined in the transverse y-z plane. The direction of magnetic field bias $\mathbf{B}_0$ is chosen to be along the z axis. (b) A linearly polarized probe beam couples to the clock transition $^1S_0$-$^3P_0$ with a bare Rabi frequency Ω_0 and detuning δ. The frequency difference induced by the gravity between two adjacent lattice sites is Δ_b. For a shallow lattice, an atom cannot be tightly confined in a single lattice site. All the field polarizations are in the z direction.

wavelength of λ_b along the vertical x axis. The typical length of 1D lattice region is $L = 10^2$ μm corresponding to about 5×10^2 lattice sites. Due to a negative dynamic polarizability of the atom in a BD dipole trap and the inhomogeneity of the lattice intensity in the y-z plane, atoms cannot be confined in the transverse direction only by the lattice field, for which we apply another RD traveling beam with a magic wavelength λ_r to overlap the BD lattice in the x direction, as shown in Fig. 1(a). The waist radium $w_{s,r}$ of the RD beam is much smaller than that of the BD lattice beam $w_{s,b}$. Thus, one can ignore the inhomogeneity of lattice beam in the y-z plane within an area of $\pi w_{s,r}^2$, and atoms can be trapped in the transverse direction via the RD traveling beam. On the other hand, due to the shallow lattice potential, an atom can tunnel to the neighboring lattice sites [as shown in Fig. 1(b)], which induces the extra intersite collisions among atoms in different lattice sites besides the two-body interactions of atoms in the same lattice site.

Here we follow a method similar to the many-body treatment of the collisional shift developed in Ref. [29]. The Hamiltonian describing cold polarized fermionic alkaline-earth-metal atoms with an s-wave interaction in a 1D optical lattice is given by [30]

$$H = \sum_{\alpha=e,g} \int d^3\mathbf{r} \Psi_\alpha^\dagger(\mathbf{r}) \left(-\frac{\hbar^2}{2m_a}\nabla^2 + U(\mathbf{r}) \right) \Psi_\alpha(\mathbf{r}) + \frac{\hbar\omega_a}{2} \int d^3\mathbf{r} [\rho_e(\mathbf{r}) - \rho_g(\mathbf{r})] + \frac{4\pi\hbar^2}{m_a} a_{eg}^- \int d^3\mathbf{r} \rho_e(\mathbf{r}) \rho_g(\mathbf{r}) - \frac{\hbar\Omega_0}{2} \int d^3\mathbf{r} \left[\Psi_e^\dagger(\mathbf{r}) e^{i\mathbf{k}_L\cdot\mathbf{r} - i\omega_L t} \Psi_g(\mathbf{r}) + \text{H.c.} \right], \quad (1)$$

where the density operator $\rho_\alpha(\mathbf{r}) = \Psi_\alpha^\dagger(\mathbf{r})\Psi_\alpha(\mathbf{r})$ and m_a is the atomic mass. The fermionic field operator $\Psi_\alpha^\dagger(\mathbf{r})$ creates a ^{87}Sr atom in the electronic state $\alpha = g$ ($^1S_0$) or e ($^3P_0$) at position $\mathbf{r}$. The first term on the right side of Eq. (1) describes the external dynamics of atoms in an optical potential combining gravity [31]

$$U(\mathbf{r}) = U_{0,b} \cos^2(k_b x) \exp\left[-2\left(y^2 + z^2\right)/w_{s,b}^2 \right] + m_a g x + U_{0,r} \exp\left[-2(y^2 + z^2)/w_{s,r}^2 \right],$$

where g is the acceleration of Earth's gravity, k_b is the wave vector of the lattice field, and $U_{0,b}$ and $U_{0,r}$ are the dipole trap potentials of the BD and RD laser fields, respectively. The second term is the Hamiltonian of the internal dynamics of free atoms. The third term describes the collision between two atoms in the antisymmetric electronic state $|-\rangle = (|ge\rangle - |eg\rangle)/\sqrt{2}$ with a scattering length a_{eg}^-. The last term denotes the atom-field interaction between the clock transition (frequency ω_a) and the probe beam (frequency ω_L and wave vector $\mathbf{k}_L$) with a corresponding bare Rabi frequency Ω_0 and the detuning $\delta = \omega_L - \omega_a$.

B. External dynamics of atom

We consider the external dynamics of an atom in a BD optical lattice. In the vertical x direction, atoms move in a periodic optical potential combining an accelerated potential, which can be described by a Hamiltonian density $h_V(x) \approx -\frac{\hbar^2}{2m_a}\partial_x^2 + U_{0,b}\cos^2(k_b x) + m_a g x$. The existence of gravity strongly suppresses the intersite tunneling effect resulting in a separation of a lattice band into isolated sites, which is called the Wannier-Stark ladder. We assume all atoms are in the bottom energy band. Two adjacent lattice sites are then shifted in energy by $\Delta_b = m_a g \lambda_b/(2\hbar) = 2\pi \times 416.5$ Hz for ^{87}Sr. Following the method in Ref. [28], one can derive the metastable Wannier-Stark state $\Phi_j(x)$ of an atom at the jth lattice site.

Figure 2(a) displays the spatial distribution of an atom moving about the 0th lattice site for different lattice potentials. The atom is tightly confined at the center of a single lattice site for a sufficiently large trap potential, for which the atomic state can be approximately described by a Gaussian function (i.e., the zeroth-order eigenfunction of a harmonic potential). However, atoms can tunnel into the neighboring sites for a lower lattice potential. As shown in Fig. 2(b), the curvature of the ground band increases as the lattice potential being decreased, which leads a large Doppler broadening and, as a result, a large-scale spatial distribution of the atom and a strong tunneling effect.

Figure 3 shows the longitudinal sideband spectra of lattice trapped atoms, where we do not include the effect of the transverse motional states. The magnitude of sidebands is proportional to the atomic tunneling effect, which can be suppressed down to 10% of the carrier magnitude for a lattice potential of $U_{0,b} = 15E_b$. Due to

$$\frac{E_b/\Delta_b}{E_r/\Delta_r} \approx 9,$$

where $E_r = 8\pi^2\hbar^2/(m_a\lambda_r^2)$ is the recoil energy of a RD photon, this minima lattice potential required to tightly confine atoms

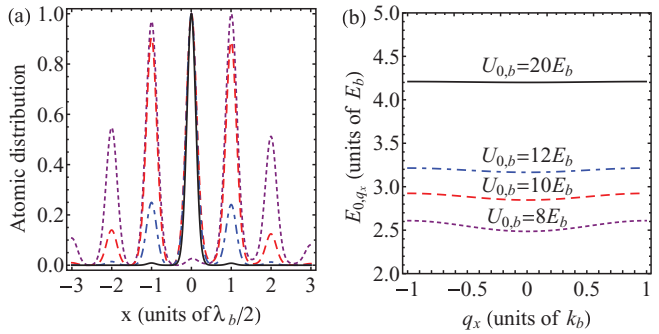

FIG. 2. (Color online) (a) The normalized spatial distribution of single ^{87}Sr atom in a 1D BD optical lattice combining an accelerated potential for different lattice trap depths. (b) The corresponding bottom energy bands E_{0,q_x} for different lattice potentials as a function of the atomic momentum q_x in the x direction. Curves with same style in both figures correspond to the same lattice potential. $E_b = 8\pi^2\hbar^2/(m_a\lambda_b^2)$ is the recoil energy of a BD photon.

in each single BD lattice site is much larger than that for a RD lattice (i.e., $5E_r$ as estimated in Ref. [28]). Here we should note that, for a typical intensity of the lattice field of 10 kW/cm^2, the BD lattice potential is about $56.4E_b$ (41 μK). In this paper, we only consider the BD lattice with a potential smaller than this value.

In the transverse y-z plane, the confinement on atoms is realized by an isotropic 2D harmonic potential, for which the atomic dynamics is approximately described by a Hamiltonian density

$$h_T(y,z) \approx -\frac{\hbar^2}{2m_a}\left(\partial_y^2+\partial_z^2\right)+U_{0,r}\frac{2(y^2+z^2)}{w_{s,r}^2}$$

for $|y|,|z| \ll w_{s,r}$. Here we have omitted the influence of the inhomogeneity of the BD field intensity in the transverse plane on the atomic external dynamics since its beam waist $w_{s,b}$ is much larger than that of the RD traveling wave $w_{s,r}$. The transverse harmonic eigenmodes can be expressed as

$$\phi_{\nu_\beta}(\beta) = \frac{e^{-\beta^2/(2\beta_0^2)}}{\pi^{1/4}\sqrt{2^{\nu_\beta}\beta_0\nu_\beta!}}H_{\nu_\beta}(\beta/\beta_0),$$

where the integral number $\nu_\beta = 0,1,\ldots,\ \beta = y,z,\ H_n$ is the nth-order Hermite polynomial, the characteristic length

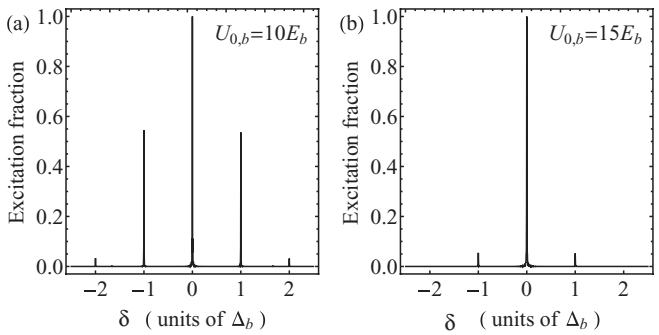

FIG. 3. Longitudinal sideband spectra with all atoms initially prepared in ground state $|g\rangle$. The effective Rabi frequency is about $2\pi \times 1.2$ Hz and the Rabi pulse duration is 424 ms.

$\beta_0 \equiv \sqrt{\hbar/(m_a\omega_\beta)}$, and the frequency of harmonic oscillator is ω_β. One can expand the field operator $\Psi_\alpha(\mathbf{r})$ in the harmonic oscillator eigenmodes and the Wannier-Stark states, $\Psi_\alpha(\mathbf{r}) = \sum_{\boldsymbol{\nu},j} c_{\alpha,\boldsymbol{\nu},j}\Phi_j(x)\phi_{\nu_y}(y)\phi_{\nu_z}(z)$, where the annihilation operator $c_{\alpha,\boldsymbol{\nu},j}$ reduces a fermion in the electronic state $|\alpha\rangle$ and transverse modes $\boldsymbol{\nu} = (\nu_y,\nu_z)$ at the jth lattice site.

As we know, the initially spin-polarized identical fermions are immune to the s-wave ultracold collisions. However, here we assume that the probe beam is slightly misaligned in the x axis with a small component along the z direction: $\mathbf{k}_L = k_{L,x}\mathbf{e}_X + k_{L,z}\mathbf{e}_Z$ ($|k_{L,z}/k_{L,x}| \ll 1$), which leads to an inhomogeneous excitation during the measurement process. In this case, the previously indistinguishable fermions become slightly distinguishable, which results in a density-dependent frequency shift. Typically, the effective misalignment angle of the probe beam with respect to the lattice axis is about $\Delta\theta \sim 10$ mrad [11].

The coupling coefficients of the atom-field interaction in the vertical and transverse directions are given by

$$\varepsilon_{j,j'} \equiv \int \Phi_j^*(x)e^{ik_{L,x}x}\Phi_{j'}(x)dx,$$
$$\varepsilon_{\nu_z,\nu_z'} \equiv \int \phi_{\nu_z}^*(z)e^{ik_{L,z}z}\phi_{\nu_z'}(z)dz,$$

respectively, which can be further approximated as $\varepsilon_{\nu_z} \approx L_{\nu_z}(\eta_z^2)e^{-\eta_z^2/2}$ if the transverse sideband transitions are negligible [29], where L_n is the Laguerre polynomial and the Lamb-Dicke parameter η_z is defined as $\eta_z \equiv k_{L,z}\sqrt{\hbar/(2m_a\omega_z)}$. Thus, the mode-dependent Rabi frequency can be expressed as $\Omega_{\nu_z,j;\nu_z',j'} = \varepsilon_{\nu_z,\nu_z'}\varepsilon_{j,j'}\Omega_0$.

We assume that the harmonic oscillator frequencies $\omega_{\beta=y,z}$ are much larger than the Rabi frequencies $\Omega_{\nu_z,j;\nu_z',j}$, $\Omega_{\nu_z,j;\nu_z,j'\neq j}$, and $\Omega_{\nu_z,j;\nu_z'\neq\nu_z,j'\neq j}$, for which both the transverse and longitudinal sideband transitions can be neglected. Hence, Hamiltonian H can be rewritten in the rotating wave approximation (RWA) as

$$H/\hbar = -\delta\sum_{\boldsymbol{\nu},j}\rho_{e,\boldsymbol{\nu},j} + \sum_{\alpha,\boldsymbol{\nu},j}\omega_{\boldsymbol{\nu},j}\rho_{\alpha,\boldsymbol{\nu},j} - \sum_{\boldsymbol{\nu},j}\left(\frac{\Omega_{\nu_z,j}}{2}\sigma_{\boldsymbol{\nu},j}^\dagger + \text{H.c.}\right) + \frac{4\pi\hbar a_{eg}^-}{m_a}\sum_{\{\boldsymbol{\nu}_i,j_i\}}A_{\{\boldsymbol{\nu}_i,j_i\}}c_{e,\boldsymbol{\nu}_1,j_1}^\dagger c_{e,\boldsymbol{\nu}_2,j_2}c_{g,\boldsymbol{\nu}_3,j_3}^\dagger c_{g,\boldsymbol{\nu}_4,j_4}, \quad (2)$$

where the density operator $\rho_{\alpha,\boldsymbol{\nu},j} \equiv c_{\alpha,\boldsymbol{\nu},j}^\dagger c_{\alpha,\boldsymbol{\nu},j}$, the Rabi-flopping operator $\sigma_{\boldsymbol{\nu},j}^\dagger \equiv c_{e,\boldsymbol{\nu},j}^\dagger c_{g,\boldsymbol{\nu},j}$, the single particle energy $\omega_{\boldsymbol{\nu},j} = \Delta_b j + \omega_y(\nu_y+1/2) + \omega_z(\nu_z+1/2)$, and the mode overlap coefficient $A_{\{\boldsymbol{\nu}_i,j_i\}} = \prod_{\beta=y,z}[\int \phi_{\nu_{1\beta}}^*(\beta)\phi_{\nu_{2\beta}}(\beta)\phi_{\nu_{3\beta}}^*(\beta)\phi_{\nu_{4\beta}}(\beta)d\beta][\int \Phi_{j_1}^*(x)\Phi_{j_2}(x)\Phi_{j_3}^*(x)\Phi_{j_4}(x)dx]$. All the characteristics of ultracold collisions are included in $A_{\{\boldsymbol{\nu}_i,j_i\}}$.

C. Four-atom system

We first focus on a simple model: four atoms distributed in two adjacent lattice sites with each site being populated by two atoms, and all the other lattice sites are empty. This system can be exactly solved via the numerical calculation. We assume all atoms are initially prepared in the electric state $|g\rangle$.

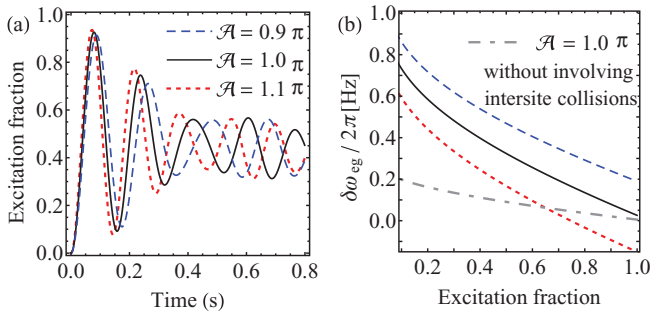

FIG. 4. (Color online) Collisional shift in four-atom system. Only two adjacent lattice sites are not empty, and each site is populated by two atoms with the initially occupied transverse modes of $\boldsymbol{\nu}_1 = (31,43)$ and $\boldsymbol{\nu}_2 = (61,71)$. (a) Rabi flopping for different Rabi pulse areas $\mathcal{A}$. (b) The collisional shift as a function of the excitation fraction for different pulse areas. The final excitation is varied by changing the detuning δ. The BD lattice potential is $U_{0,b} = 12E_b$ and the RD transverse trap depth is $U_{0,r} = -37E_r$ ($-6\ \mu$K). The beam waist of RD laser field is about $w_{s,r} = 30\ \mu$m, while that of the lattice laser is much larger than $w_{s,r}$. The s-wave scattering length $|a_{eg}^-|$ is about 200 a_0 (Bohr radii), and the time duration of a π Rabi pulse is chosen to be $t_f = 80$ ms. The typical misalignment angle of the probe beam is about $\Delta\theta \simeq 10$ mrad. Curves with the same style in both figures correspond to the same pulse area $\mathcal{A}$. The dash-dotted line in (b) denotes the collisional shift without involving the intersite collisions.

Figure 4(a) displays the Rabi flopping of four atoms between two clock-transition states for different Rabi pulse areas $\mathcal{A} = t_f\bar{\Omega}$ (t_f the time duration of a π Rabi pulse, $\bar{\Omega} = \frac{1}{4}\sum_{\boldsymbol{\nu},j}\Omega_{\boldsymbol{\nu},j}$ the average Rabi frequency, and $\Omega_{\boldsymbol{\nu},j} \equiv \Omega_{\boldsymbol{\nu},j;\boldsymbol{\nu},j}$), which quickly decays after two cycles due to the inhomogeneous excitation of the probe beam. Figure 4(b) shows the collisional shift $\delta\omega_{eg}$ of the clock-transition frequency changing with the excitation fraction for different Rabi pulse areas. As we can see, a lower excitation always leads to a larger collisional shift, and $\delta\omega_{eg}$ is sensitive to the pulse area $\mathcal{A}$. For $\mathcal{A} > \pi$, $\delta\omega_{eg}$ is positive for any excitation fraction and approaches zero only as $N_e(t_f)/N \to 1$ (N_e the number of atoms in the electric state $|e\rangle$ and N is the total atomic number) and $\mathcal{A} \to \pi$. However, $\delta\omega_{eg}$ changes sign for $\mathcal{A} < \pi$, and the zero-crossing point moves toward smaller $N_e(t_f)/N$ with the pulse area being decreased.

We also compare the collisional shift in two different cases, as shown in Fig. 4(b); that is, the case with the existence of the two-body interactions of atoms in different lattice sites and the case without involving the intersite collisions. One can see that for the higher excitation $N_e(t_f)/N \to 1$, the influence of intersite collisions on $\delta\omega_{eg}$ is weaker. However, its effect becomes more obvious for $N_e(t_f)/N \to 0$. For a clock laser whose frequency is locked at the point of $N_e(t_f)/N = 0.5$, the effect of intersite collisions should be considered carefully.

Based on this simple four-atom system, one can obtain two conclusions: (i) For two atoms in a same lattice site, only collisions with $(\boldsymbol{\nu}_2,\boldsymbol{\nu}_4) = (\boldsymbol{\nu}_1,\boldsymbol{\nu}_3)$ or $(\boldsymbol{\nu}_2,\boldsymbol{\nu}_4) = (\boldsymbol{\nu}_3,\boldsymbol{\nu}_1)$, which describe the exchange of the transverse modes, mainly contribute to the collisional frequency shift. Thus, the mode overlap coefficient can be simplified as $A^j_{\boldsymbol{\nu},\boldsymbol{\nu}'} \equiv A_{\boldsymbol{\nu},j;\boldsymbol{\nu},j;\boldsymbol{\nu}',j;\boldsymbol{\nu}',j}$ by using its symmetry [29]. (ii) For two atoms in different sites, the two-body interactions are dominated by the terms of $(j_2,j_4) = (j_1,j_3)$ or $(j_2,j_4) = (j_3,j_1)$ with the transverse modes satisfying the condition (i). The mode overlap coefficient in this case can be simplified as $A^{j,j'}_{\boldsymbol{\nu},\boldsymbol{\nu}'} \equiv A_{\boldsymbol{\nu},j;\boldsymbol{\nu},j;\boldsymbol{\nu}',j';\boldsymbol{\nu}',j'}$. Therefore, the primary collision processes conserve the number of atoms per state; that is, collisions mainly happen between two states that are initially occupied by atoms.

III. SPIN-$\frac{1}{2}$ MODEL AND COLLISIONAL SHIFT

According to the conclusions derived above, it is possible to reduce Hamiltonian H to a spin-$\frac{1}{2}$ model. We assume a set of transverse eigenmodes $\{\tilde{\boldsymbol{\nu}}(j)\}$ are initially populated by atoms, where $\tilde{\boldsymbol{\nu}}(j)$ denotes a set of the populated transverse modes in the jth lattice site. Additionally, since the mode overlap coefficients $A^j_{\boldsymbol{\nu},\boldsymbol{\nu}'}$ and $A^{j,j'}_{\boldsymbol{\nu},\boldsymbol{\nu}'}$ are the slowly varying functions of $|\nu_\beta - \nu'_\beta|$ ($\beta = y,z$), we can approximate them by their average values over all the possible collision terms; that is [29],

$$\bar{A}^j_{\tilde{\boldsymbol{\nu}}} \equiv \frac{1}{N_j^2}\sum_{\boldsymbol{\nu},\boldsymbol{\nu}'\in\tilde{\boldsymbol{\nu}}(j)} A^j_{\boldsymbol{\nu},\boldsymbol{\nu}'},$$

$$\bar{A}^{j,j'}_{\tilde{\boldsymbol{\nu}}} \equiv \frac{1}{N_j N_{j'}}\sum_{\boldsymbol{\nu}\in\tilde{\boldsymbol{\nu}}(j),\boldsymbol{\nu}'\in\tilde{\boldsymbol{\nu}}(j')} A^{j,j'}_{\boldsymbol{\nu},\boldsymbol{\nu}'},$$

where N_j is the number of atoms in the jth lattice site. On the other hand, we can divide the Rabi frequency $\Omega_{\nu_z,j}$ into a mean value $\bar{\Omega}_{\tilde{\boldsymbol{\nu}},j} = \frac{1}{N_j}\sum_{\boldsymbol{\nu}\in\tilde{\boldsymbol{\nu}}(j)}\Omega_{\nu_z,j}$ over the transverse modes $\tilde{\boldsymbol{\nu}}$ in the jth lattice site and a small difference $\delta\Omega_{\nu_z,j} = \Omega_{\nu_z,j} - \bar{\Omega}_{\tilde{\boldsymbol{\nu}},j}$, which can be considered as a perturbation.

By defining the spin operators

$$S^x_{\boldsymbol{\nu},j} \equiv \tfrac{1}{2}(c^\dagger_{e,\boldsymbol{\nu},j}c_{g,\boldsymbol{\nu},j} + c^\dagger_{g,\boldsymbol{\nu},j}c_{e,\boldsymbol{\nu},j}),$$
$$S^y_{\boldsymbol{\nu},j} \equiv \tfrac{1}{2i}(c^\dagger_{e,\boldsymbol{\nu},j}c_{g,\boldsymbol{\nu},j} - c^\dagger_{g,\boldsymbol{\nu},j}c_{e,\boldsymbol{\nu},j}),$$
$$S^z_{\boldsymbol{\nu},j} \equiv \tfrac{1}{2}(c^\dagger_{e,\boldsymbol{\nu},j}c_{e,\boldsymbol{\nu},j} - c^\dagger_{g,\boldsymbol{\nu},j}c_{g,\boldsymbol{\nu},j}),$$

Eq. (2) can be reexpressed as

$$H/\hbar = -\delta\sum_j S^z_j - \sum_j\left(\frac{\bar{\Omega}_{\tilde{\boldsymbol{\nu}},j}}{2}S^+_j + \text{H.c.}\right) - \sum_j U_{\tilde{\boldsymbol{\nu}},j}\vec{S}_j\cdot\vec{S}_j$$
$$- \sum_{\boldsymbol{\nu},j}\left(\frac{\delta\Omega_{\nu_z,j}}{2}S^+_{\boldsymbol{\nu},j} + \text{H.c.}\right) - \sum_{j,\delta j>0} V_{\tilde{\boldsymbol{\nu}},j,\delta j}\vec{S}_j\cdot\delta\vec{S}_{j,\delta j}, \tag{3}$$

where we have defined the spin vector $\vec{S}_j = S^x_j\mathbf{e}_x + S^y_j\mathbf{e}_y + S^z_j\mathbf{e}_z$, the component in each direction $S^\alpha_j = \sum_{\boldsymbol{\nu}\in\tilde{\boldsymbol{\nu}}(j)}S^\alpha_{\boldsymbol{\nu},j}$ ($\alpha = x,y,z$), the *effective* strength of interaction between two atoms in a same lattice site

$$U_{\tilde{\boldsymbol{\nu}},j} = \frac{4\pi\hbar}{m_a}a^-_{eg}\left(\bar{A}^j_{\tilde{\boldsymbol{\nu}}} + 2\sum_{\delta j>0}\bar{A}^{j,j+\delta j}_{\tilde{\boldsymbol{\nu}}}\right),$$

and the *effective* collision strength of atoms in two different lattice sites

$$V_{\boldsymbol{\nu},j,\delta j} = \frac{8\pi\hbar}{m_a}a^-_{eg}\bar{A}^{j,j+\delta j}_{\tilde{\boldsymbol{\nu}}}.$$

Since the two-body collisions do not change the number of atoms in an external atomic state as we discussed above,

the primary part of intersite collisions can be equivalently involved into the interactions of atoms in a single lattice site (i.e., the second term in the round brackets of the expression of $U_{\tilde{\boldsymbol{\nu}},j}$), which leads a spin fluctuation $\delta\vec{S}_{j,\delta j}=\frac{1}{2}(\vec{S}_{j+\delta j}+\vec{S}_{j-\delta j})-\vec{S}_j$. On the other hand, since $\bar{A}_{\tilde{\boldsymbol{\nu}}}^{j,j+\delta j}$ rapidly decreases with increasing the distance δj between two atoms, the intersite collisions, which only cover several neighboring lattice sites, mainly affect the clock-transition frequency shift.

A. Hamiltonian in rotated frame

For simplicity we express Hamiltonian H in a rotated frame. Based on the real and imaginary parts of the averaged Rabi frequency $\bar{\Omega}_{\tilde{\boldsymbol{\nu}},j}$ [i.e., $\bar{\Omega}^r_{\tilde{\boldsymbol{\nu}},j}=\frac{1}{2}(\bar{\Omega}_{\tilde{\boldsymbol{\nu}},j}+\bar{\Omega}^*_{\tilde{\boldsymbol{\nu}},j})$ and $\bar{\Omega}^i_{\tilde{\boldsymbol{\nu}},j}=\frac{1}{2i}(\bar{\Omega}_{\tilde{\boldsymbol{\nu}},j}-\bar{\Omega}^*_{\tilde{\boldsymbol{\nu}},j})$] and the detuning δ of the probe beam, one can define a unit vector $\boldsymbol{\epsilon}_{\tilde{\boldsymbol{\nu}},j}=\epsilon^x_{\tilde{\boldsymbol{\nu}},j}\mathbf{e}_x+\epsilon^y_{\tilde{\boldsymbol{\nu}},j}\mathbf{e}_y+\epsilon^z_{\tilde{\boldsymbol{\nu}},j}\mathbf{e}_z$, where the three components are $\epsilon^x_{\tilde{\boldsymbol{\nu}},j}=\bar{\Omega}^r_{\tilde{\boldsymbol{\nu}},j}/\omega_{\tilde{\boldsymbol{\nu}},j}$, $\epsilon^y_{\tilde{\boldsymbol{\nu}},j}=\bar{\Omega}^i_{\tilde{\boldsymbol{\nu}},j}/\omega_{\tilde{\boldsymbol{\nu}},j}$, $\epsilon^z_{\tilde{\boldsymbol{\nu}},j}=\delta/\omega_{\tilde{\boldsymbol{\nu}},j}$, and the total frequency $\omega_{\tilde{\boldsymbol{\nu}},j}=\sqrt{(\bar{\Omega}^r_{\tilde{\boldsymbol{\nu}},j})^2+(\bar{\Omega}^i_{\tilde{\boldsymbol{\nu}},j})^2+\delta^2}$. By choosing the vector $\boldsymbol{\epsilon}$ as a new rotation axis (a new z direction), we can define a new spin vector $\vec{s}_{\boldsymbol{\nu},j}=s^x_{\boldsymbol{\nu},j}\mathbf{e}_x+s^y_{\boldsymbol{\nu},j}\mathbf{e}_y+s^z_{\boldsymbol{\nu},j}\mathbf{e}_z$ with the three components being expressed as

$$
\begin{aligned}
s^x_{\boldsymbol{\nu},j}&=\cos\phi_{\tilde{\boldsymbol{\nu}},j}\cos\theta_{\tilde{\boldsymbol{\nu}},j}S^x_{\boldsymbol{\nu},j}-\sin\phi_{\tilde{\boldsymbol{\nu}},j}\cos\theta_{\tilde{\boldsymbol{\nu}},j}S^y_{\boldsymbol{\nu},j}+\sin\theta_{\tilde{\boldsymbol{\nu}},j}S^z_{\boldsymbol{\nu},j},\\
s^y_{\boldsymbol{\nu},j}&=\sin\phi_{\tilde{\boldsymbol{\nu}},j}S^x_{\boldsymbol{\nu},j}+\cos\phi_{\tilde{\boldsymbol{\nu}},j}S^y_{\boldsymbol{\nu},j},\\
s^z_{\boldsymbol{\nu},j}&=-\cos\phi_{\tilde{\boldsymbol{\nu}},j}\sin\theta_{\tilde{\boldsymbol{\nu}},j}S^x_{\boldsymbol{\nu},j}+\sin\phi_{\tilde{\boldsymbol{\nu}},j}\sin\theta_{\tilde{\boldsymbol{\nu}},j}S^y_{\boldsymbol{\nu},j}+\cos\theta_{\tilde{\boldsymbol{\nu}},j}S^z_{\boldsymbol{\nu},j},
\end{aligned}
$$

where the rotation angles $\theta_{\tilde{\boldsymbol{\nu}},j}$ and $\phi_{\tilde{\boldsymbol{\nu}},j}$ can be derived from

$$
\cos\theta_{\tilde{\boldsymbol{\nu}},j}=\epsilon^z_{\tilde{\boldsymbol{\nu}},j},\quad \sin\theta_{\tilde{\boldsymbol{\nu}},j}=\sqrt{\left(\epsilon^x_{\tilde{\boldsymbol{\nu}},j}\right)^2+\left(\epsilon^y_{\tilde{\boldsymbol{\nu}},j}\right)^2},
$$
$$
\cos\phi_{\tilde{\boldsymbol{\nu}},j}=\frac{\epsilon^x_{\tilde{\boldsymbol{\nu}},j}}{\sin\theta_{\tilde{\boldsymbol{\nu}},j}},\quad \sin\phi_{\tilde{\boldsymbol{\nu}},j}=-\frac{\epsilon^y_{\tilde{\boldsymbol{\nu}},j}}{\sin\theta_{\tilde{\boldsymbol{\nu}},j}}.
$$

One can show that $\vec{s}_j^{\,2}=\vec{S}_j^2$ and $\vec{s}_j\cdot\delta\vec{s}_{j,\delta j}=\vec{S}_j\cdot\delta\vec{S}_{j,\delta j}$, where $\vec{s}_j=\sum_{\boldsymbol{\nu}\in\tilde{\boldsymbol{\nu}}(j)}\vec{s}_{\boldsymbol{\nu},j}$.

Similar to the averaged Rabi frequency $\bar{\Omega}_{\tilde{\boldsymbol{\nu}},j}$, the real and imaginary parts of the tiny Rabi frequency difference $\delta\Omega_{\nu_z,j}$ are given by $\delta\Omega^r_{\nu_z,j}=\frac{1}{2}(\delta\Omega_{\nu_z,j}+\delta\Omega^*_{\nu_z,j})$ and $\delta\Omega^i_{\nu_z,j}=\frac{1}{2i}(\delta\Omega_{\nu_z,j}-\delta\Omega^*_{\nu_z,j})$, respectively. In the rotated frame, $\delta\Omega_{\nu_z,j}$ should be changed to $(\delta\Omega^x_{\nu_z,j},\delta\Omega^y_{\nu_z,j},\delta\Omega^z_{\nu_z,j})$, where

$$
\begin{aligned}
\delta\Omega^x_{\nu_z,j}&=\left(\delta\Omega^r_{\nu_z,j}\cos\phi_{\tilde{\boldsymbol{\nu}},j}+\delta\Omega^i_{\nu_z,j}\sin\phi_{\tilde{\boldsymbol{\nu}},j}\right)\cos\theta_{\tilde{\boldsymbol{\nu}},j},\\
\delta\Omega^y_{\nu_z,j}&=\delta\Omega^r_{\nu_z,j}\sin\phi_{\tilde{\boldsymbol{\nu}},j}-\delta\Omega^i_{\nu_z,j}\cos\phi_{\tilde{\boldsymbol{\nu}},j},\\
\delta\Omega^z_{\nu_z,j}&=-\left(\delta\Omega^r_{\nu_z,j}\cos\phi_{\tilde{\boldsymbol{\nu}},j}+\delta\Omega^i_{\nu_z,j}\sin\phi_{\tilde{\boldsymbol{\nu}},j}\right)\sin\theta_{\tilde{\boldsymbol{\nu}},j}.
\end{aligned}
$$

Based on the expressions of the new spin vector $\vec{s}_{\boldsymbol{\nu},j}$ and Rabi frequency differences $\delta\Omega^\alpha_{\nu_z,j}$ ($\alpha=x,y,z$), Hamiltonian (3) can be rewritten in a simple form

$$
\begin{aligned}
H/\hbar=&-\sum_j\omega_{\tilde{\boldsymbol{\nu}},j}s^z_j-\sum_j U_{\tilde{\boldsymbol{\nu}},j}\vec{s}_j\cdot\vec{s}_j-\sum_{\alpha,\boldsymbol{\nu},j}\delta\Omega^\alpha_{\nu_z,j}s^\alpha_{\boldsymbol{\nu},j}\\
&-\sum_{j,\delta j}V_{\tilde{\boldsymbol{\nu}},j,\delta j}\vec{s}_j\cdot\delta\vec{s}_{j,\delta j},
\end{aligned}
\tag{4}
$$

which is the basis of the following discussion. In the case of a homogeneous excitation ($\delta\Omega^\alpha_{\tilde{\boldsymbol{\nu}},j}=0$), $\vec{s}_j^{\,2}$ and s^z_j are two conserved quantities. The system will be only in the $s_j=N_j/2$ manifold and no collision-induced frequency shift exists because the Pauli exclusion principle ensures the maintenance of the initial zero s-wave interaction [32]. On the other hand, for a sufficiently large lattice potential, the intersite collisions can be sufficiently suppressed (i.e., $\bar{A}_{\tilde{\boldsymbol{\nu}}}^{j,j+\delta j}\to 0$), and one can ignore its influence on the clock-transition frequency shift.

Initially, all the atoms are prepared in the ground electric state $|g\rangle$. For a fixed set of the populated transverse modes $\tilde{\boldsymbol{\nu}}(j)$ in the jth lattice site, the atomic state at time $t=0$ can be expressed as $|\psi_{\tilde{\boldsymbol{\nu}},j}(t=0)\rangle=|\frac{N_j}{2},-\frac{N_j}{2}\rangle$ in the spin momentum representation. Furthermore, by applying the Wigner rotation matrices one can obtain the initial state

$$
\begin{aligned}
&|\psi_{\tilde{\boldsymbol{\nu}},j}(t=0)\rangle\\
&=\sum_{m_j=-N_j/2}^{N_j/2}e^{-im_j\phi_{\tilde{\boldsymbol{\nu}},j}}\left[\frac{N_j!}{(N_j/2-m_j)!(N_j/2+m_j)!}\right]^{1/2}\\
&\quad\times\cos^{N_j/2-m_j}\left(\frac{\theta_{\tilde{\boldsymbol{\nu}},j}}{2}\right)\sin^{N_j/2+m_j}\left(\frac{\theta_{\tilde{\boldsymbol{\nu}},j}}{2}\right)|N_j/2,m_j\rangle
\end{aligned}
$$

in the rotated spin momentum space.

B. Perturbations in the spin-$\frac{1}{2}$ model

In the presence of the excitation inhomogeneity ($\delta\Omega^\alpha_{\boldsymbol{\nu},j}\neq 0$), $\vec{s}_j^{\,2}$ are no longer conserved, and more manifolds should be involved. However, according to the conclusion in Ref. [29], since the misalignment of the probe beam is slight, the third term in Eq. (4) can be viewed as a perturbation. To first order in perturbation theory, it is enough to consider the transition within the $s_j=\frac{N_j}{2}$ and $\frac{N_j}{2}-1$ manifolds.

Now we prove that the fourth term in Eq. (4) is a perturbation. If $|V_{\tilde{\boldsymbol{\nu}},j,\delta j}|$ is much smaller than $|U_{\tilde{\boldsymbol{\nu}},j}|$, it is natural to view $V_{\tilde{\boldsymbol{\nu}},j,\delta j}\vec{s}_j\cdot\delta\vec{s}_{j,\delta j}$ as a perturbation of $U_{\tilde{\boldsymbol{\nu}},j}\vec{s}_j\cdot\vec{s}_j$. But $|V_{\tilde{\boldsymbol{\nu}},j,\delta j}|\ll|U_{\tilde{\boldsymbol{\nu}},j}|$ is not a necessary condition. Since the Rabi flopping during the time interval ($0\sim t_f$) is mainly determined by the homogeneous excitation, we can only compare the average values of $U_{\tilde{\boldsymbol{\nu}},j}\langle\vec{s}_j\cdot\vec{s}_j\rangle$ and $V_{\tilde{\boldsymbol{\nu}},j,\delta j}\langle\vec{s}_j\cdot\delta\vec{s}_{j,\delta j}\rangle$ based on the zeroth-order wave functions (i.e., $\delta\Omega^\alpha_{\boldsymbol{\nu},j}=0$), and it is easily to obtain

$$
\left\|\frac{V_{\tilde{\boldsymbol{\nu}},j,\delta j}\langle\vec{s}_j\cdot\delta\vec{s}_{j,\delta j}\rangle}{U_{\tilde{\boldsymbol{\nu}},j}\langle\vec{s}_j\cdot\vec{s}_j\rangle}\right\|\approx\left\|\frac{V_{\tilde{\boldsymbol{\nu}},j,\delta j}}{U_{\tilde{\boldsymbol{\nu}},j}}\frac{N_{j-\delta j}+N_{j+\delta j}-2N_j}{N_j}\right\|
$$

for $N_j\gg 1$. Here, $\langle\cdots\rangle$ denotes the quantum average over all the possible spin states. Typically, $N_j\gg|N_j-N_{j-\delta j}|$, $|N_j-N_{j+\delta j}|$, and $|V_{\tilde{\boldsymbol{\nu}},j}|<|U_{\tilde{\boldsymbol{\nu}},j}|$. Therefore, the last term in Eq. (4) can be viewed as a perturbation compared with the second term. On the other hand, we can view $\delta\vec{s}_{j,\delta j}$ as a perturbation compared with $\vec{s}_j$ for reasons that (i) the homogeneous excitation dominates the Rabi flopping during the time interval ($0\sim t_f$) and (ii) the averaged atomic number slowly varies along the lattice axis. To a good approximation, one can use the zeroth-order value of $\delta\vec{s}_{j,\delta j}$ for the calculation of the collisional shift.

C. Expression of collisional shift

Since collisions do not change the number of atoms in each lattice site, we can express the time-evolving many-body state of the whole system $|\psi_{\{\boldsymbol{\nu}(j)\}}(t)\rangle \equiv \prod_j |\psi_{\boldsymbol{\nu},j}(t)\rangle$ as

$$|\psi_{\{\boldsymbol{\nu}(j)\}}(t)\rangle = \prod_j \left(\sum_{m_j} c_{m_j}(t) e^{-i\omega_{N_j/2,m_j} t} |N_j/2, m_j\rangle + \sum_{m_j,k_j} b_{m_j,k_j}(t) e^{-i\omega_{N_j/2-1,m_j} t} |N_j/2-1, m_j, k_j\rangle \right),$$

where the eigenfrequencies

$$\omega_{N_j/2,m_j} = m_j \omega_{\tilde{\boldsymbol{\nu}},j} - \frac{U_{\tilde{\boldsymbol{\nu}},j}}{2}\frac{N_j}{2}\left(\frac{N_j}{2}+1\right),$$

$$\omega_{N_j/2-1,m_j} = m_j \omega_{\tilde{\boldsymbol{\nu}},j} - \frac{U_{\tilde{\boldsymbol{\nu}},j}}{2}\frac{N_j}{2}\left(\frac{N_j}{2}-1\right).$$

The normalization of amplitudes c_{m_j} and b_{m_j,k_j} are given by $\sum_{m_j} |c_{m_j}(t)|^2 + \sum_{m_j,k_j} |b_{m_j,k_j}(t)|^2 = 1$.

In order to determine the time-dependent coefficients $c_{m_j}(t)$ and $b_{m_j,k_j}(t)$, we begin by writing a perturbation expansion for the coefficients, $c_{m_j}(t) \approx c^{(0)}_{m_j}(t) + c^{(1)}_{m_j}(t) + c^{(2)}_{m_j}(t)$ and $b_{m_j,k_j}(t) \approx b^{(0)}_{m_j,k_j}(t) + b^{(1)}_{m_j,k_j}(t) + b^{(2)}_{m_j,k_j}(t)$. Since atoms are all prepared in the ground state initially, we have $c^{(0)}_{m_j}(t) = c^{(0)}_{m_j}(0)$, $b^{(0)}_{m_j,k_j}(t) = 0$, and $\sum_{m_j} |c^{(0)}_{m_j}(0)|^2 = N_j$. According to the Schrödinger equation $i\hbar \frac{\partial}{\partial t} |\psi_{\{\boldsymbol{\nu}(j)\}}(t)\rangle = H |\psi_{\{\boldsymbol{\nu}(j)\}}(t)\rangle$ and time-dependent perturbation theory, one can derive the expressions of coefficients $c^{(1)}_{m_j}$ and $c^{(2)}$ and $b^{(1)}_{m_j,k_j}$ and $b^{(2)}_{m_j,k_j}$. Besides the required transition matrix elements for the perturbative calculations, which have already been given in Ref. [21], some other formulas should be applied; namely,

$$\sum_{n=1}^{N_j} e^{-i2\pi k_j n/N_j} = 0,$$

$$\sum_{k_j=1}^{N_j-1} e^{-i2\pi k_j n/N_j} = -1,$$

$$\sum_{k_j=1}^{N_j-1}\sum_{n=1}^{N_j} \delta\Omega^{\alpha}_{n,j} e^{-i2\pi k_j n/N_j} = 0,$$

$$\sum_{n,n'=1}^{N_j} \delta\Omega^{\alpha}_{n',j}\delta\Omega^{\alpha}_{n,j} e^{-i2\pi k_j (n'-n)/N_j} = N_j \sum_{n=1}^{N_j} \left(\delta\Omega^{\alpha}_{n,j}\right)^2.$$

For a set of the populated transverse states $\{\tilde{\boldsymbol{\nu}}(j)\}$, the time-dependent population in the excited state can be expressed as

$$N^{e}_{\{\tilde{\boldsymbol{\nu}}(j)\}}(t) = \sum_j \left(\frac{N_j}{2} + \langle S^z_{\tilde{\boldsymbol{\nu}},j}(t)\rangle\right) = \sum_j \left(\frac{N_j}{2} + \sin\theta_{\tilde{\boldsymbol{\nu}},j}\langle s^x_{\tilde{\boldsymbol{\nu}},j}(t)\rangle + \cos\theta_{\tilde{\boldsymbol{\nu}},j}\langle s^z_{\tilde{\boldsymbol{\nu}},j}(t)\rangle\right)$$

by applying the expression of the many-body state $|\psi_{\{\boldsymbol{\nu}(j)\}}(t)\rangle$. After some algebra, one can show that $N^{e}_{\{\tilde{\boldsymbol{\nu}},j\}}(t)$ depends on $\Omega_{\nu_z,j}$ only through the mean Rabi frequency $\bar{\Omega}_{\tilde{\boldsymbol{\nu}},j}$ of the jth lattice site and the standard deviation of Rabi frequency $\Delta\Omega_{\tilde{\boldsymbol{\nu}},j} = \sqrt{\frac{1}{N_j}\sum_{\boldsymbol{\nu}}(\Omega_{\nu_z,j} - \bar{\Omega}_{\tilde{\boldsymbol{\nu}},j})^2}$. The collisional shift is measured by locking the laser frequency at two points of equal height in the clock-transition line shape and can be expressed as [29]

$$\delta\omega_{eg} = \frac{N^{e}_{\{\tilde{\boldsymbol{\nu}},j\}}(t_f,\delta_0) - N^{e}_{\{\tilde{\boldsymbol{\nu}},j\}}(t_f,-\delta_0)}{2\partial N^{e,(0)}_{\{\tilde{\boldsymbol{\nu}},j\}}(t_f,\delta)/\partial\delta\big|_{\delta=\delta_0}}, \tag{5}$$

where the superscript (0) denotes a homogeneous excitation (i.e., $\delta\Omega^{\alpha}_{\nu_z,j} = 0$). Due to $\langle N_j/2, m_j|s^{x,y,z}_j|N_j/2-1, m'_j, k_j\rangle = 0$, $\delta\omega_{eg}$ does not have the first-order correction related to $\Delta\Omega_{\tilde{\boldsymbol{\nu}},j}$.

So far we have assumed a fixed set of populated transverse eigenstates $\{\tilde{\boldsymbol{\nu}}(j)\}$. At finite temperature T, the quantities $U_{\tilde{\boldsymbol{\nu}},j}$, $V_{\tilde{\boldsymbol{\nu}},j,\delta j}$, $\Omega_{\tilde{\boldsymbol{\nu}},j}$, and $\delta\Omega^{\alpha}_{\nu_z,j}$ should be thermally averaged; that is,

$$\langle O\rangle_T = \frac{\sum_{\tilde{\boldsymbol{\nu}}} O(\tilde{\boldsymbol{\nu}}) e^{-E(\tilde{\boldsymbol{\nu}})/(k_B T)}}{\sum_{\tilde{\boldsymbol{\nu}}} e^{-E(\tilde{\boldsymbol{\nu}})/(k_B T)}}.$$

Here we can express the two-body interaction strength $\langle U_{\tilde{\boldsymbol{\nu}},j}\rangle_T$ as $\langle U\rangle_T = u\xi^2_T$, where the thermal-independent part is

$$u = 4\pi a^{-}_{eg}\sqrt{\omega_y\omega_z}\int |\Phi_0(x)|^2 \left(|\Phi_0(x)|^2 + \sum_{\delta j>0} 2|\Phi_{\delta j}(x)|^2\right) dx \tag{6}$$

and the temperature-dependent dimensionless parameter

$$\xi = \left\langle \int \frac{d\beta}{\beta_0} \left|\phi_{\nu_\beta}(\beta)\phi_{\nu'_\beta}(\beta)\right|^2 \right\rangle_{a,T}.$$

The notation $\langle\cdots\rangle_{a,T}$ denotes an average over the different transverse eigenmodes combing the thermal average.

D. Collisional shift in 1D BD lattice

We assume that the number of atoms loaded into a single lattice site obeys a Poissonian probability distribution with a mean value determined by the assumed distribution of atoms $\bar{N}_j = \frac{N}{\sqrt{2\pi\tilde{\sigma}^2}} \exp[-j^2/(2\tilde{\sigma}^2)]$, where $\tilde{\sigma} = 2w_{s,r}/\lambda_b$ is the standard deviation of the Gaussian distribution in units of the lattice constant $\lambda_b/2$ and N is the total number of atoms trapped in lattice region [24].

Figure 5(a) displays the strength u of the two-body interaction changing with the lattice potential. One can see that, for a shallow optical lattice, the intersite interactions can surpass the collisions of atoms in a single lattice site and primarily contribute to the clock-transition frequency shift [Fig. 5(b)], which coincides with the spatial distribution of atom shown in Fig. 2(a). Increasing the lattice potential can suppress the intersite collisions, but it also increases the collisional shift since the strength of the two-body interaction is in a weakly interacting regime ($u \ll \langle\Omega\rangle_T$). For $U_{0,b} > 15E_b$, the collision-induced frequency shift is mainly affected by the collisions of atoms at a single lattice site. For our system, the minimal lattice potential required to sufficiently suppress the intersite collisions is about $15E_b$ (14.5 μK), which is much larger than that required for a RD lattice. This is because λ_r is about two times larger than λ_b, which leads to $E_b \approx 4.35E_r$ and $\Delta_r \approx 2.1\Delta_b$. If the frequency of a local oscillator is

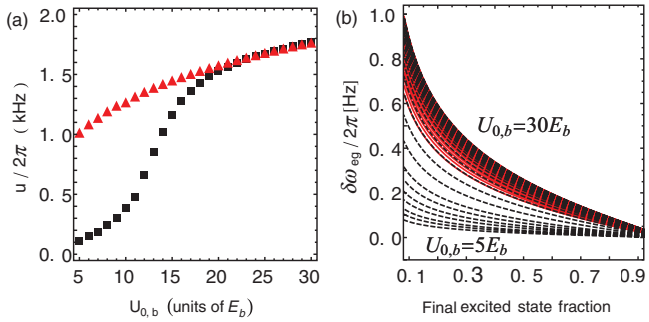

FIG. 5. (Color online) (a) Interaction strength u as a function of lattice potential with (triangles) and without (squares) involving the intersite collisions. (b) Collisional shift changing with final excited-state fraction for different lattice potentials. The lattice potential is increased from $5E_b$ to $30E_b$ with each step of E_b. Solid lines: $\delta\omega_{eg}$ including the intersite interactions. Dashed lines: $\delta\omega_{eg}$ without involving the intersite collisions. For both figures, the atomic temperature is about $T = 3\ \mu$K and the atomic number is $N = 3000$. All the other parameters are the same as for Fig. 4.

phase locked at the half-height point of the clock-transition spectrum ($N_e \sim N_g$, where $N_{\alpha=e,g}$ is the total number of atoms in the electric state $|\alpha\rangle$), the fractional collisional shift is about $\delta\omega_{eg}/\omega_a \approx 4.6 \times 10^{-16}$ for a lattice potential of $U_{0,b} = 15E_b$.

Since each lattice site traps a different number of atoms, the collisional shifts in different single lattice sites vary over the whole lattice region. This inhomogeneity, which is caused by the atomic distribution, decreases for higher excitations, as shown in Fig. 6(a), because all the collisional shifts should approach zero as $N_e(t_f)/N \to 1$. In addition, this inhomogeneity introduces an extra statistical uncertainty into the phase locking of a local oscillator because a different collisional shift is involved in each interrogation. Reducing the number of atoms trapped in each lattice site can suppress this kind of inhomogeneous frequency shift, which, however, decreases the signal-to-noise ratio. Thus, a 2D optical lattice is a better choice since the number of atoms in each lattice site can be reduced to less than two but a large number of quantum absorbers still remain.

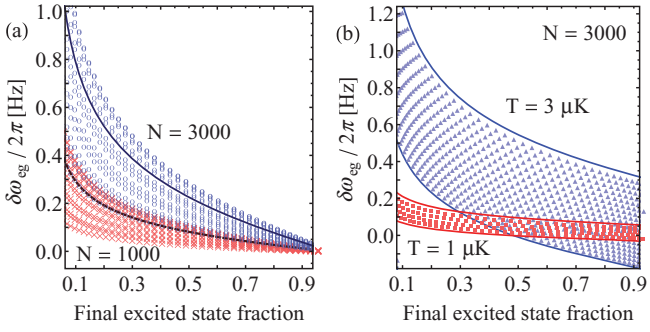

FIG. 6. (Color online) (a) Collisional shifts for different numbers of atoms with shaded area denoting frequency shifts in each single lattice site. The temperature of atoms is $T = 3\ \mu$K. (b) Collisional shifts for different atomic temperature with a ~10% variation of the π Rabi pulse area $\mathcal{A}$. All the other parameters are the same as for Fig. 4.

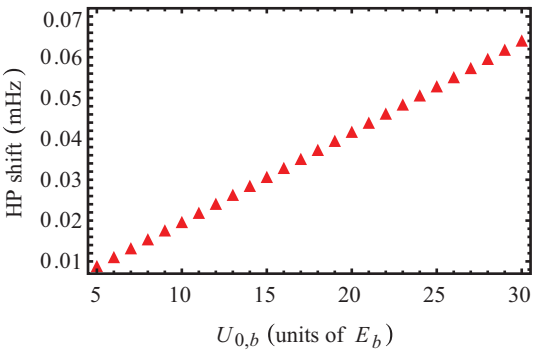

FIG. 7. (Color online) HP shift in 1D BD lattice as a function of lattice potential $U_{0,b}$.

Figure 6(b) shows the collisional shift for different atomic temperatures. Reducing the atomic temperature can decrease the number of transverse eigenmodes possibly populated by atoms. As a result, the inhomogeneous excitation can be suppressed, and hence the collisional shift is reduced. On the other hand, due to a ~10% variance of the π Rabi pulse area $\mathcal{A}$ in experiment, the collisional shift distributes in a band area. Reducing the temperature of atoms can also decrease the influence of the variance of $\mathcal{A}$.

Figure 7 displays the hyperpolarizability (HP) shift in a BD lattice changing with lattice potential, where we have used the fact that the difference between HPs of the upper and lower clock levels is about $\Delta\beta = 0.1$ mHz/(kW/cm^2)^2 at λ_b [26]. Since atoms are trapped in the intensity minima of the lattice field and because we choose a shallow optical lattice here, the higher-order light shift can be quite a bit smaller than 1 mHz, which is attractive to realize a high-performance optical clock.

IV. SPIN-POLARIZED ATOMS IN 2D OPTICAL LATTICE

Above we have considered the effect of intersite collisions on the collision-induced frequency shift in a 1D optical lattice. As demonstrated in Ref. [21], by tightly confining atoms in a 2D lattice, the two-body interaction energy u can exceed the thermally averaged Rabi frequency $\langle\Omega\rangle_T$, which significantly suppresses the transition between the atomic singlet and triplet states and results in a reduction in collisional shift. In this section, we consider an ensemble of spin-polarized ^{87}Sr ($I = 9/2$) atoms trapped in a 2D BD optical lattice, as shown in Fig. 8. A 2D array of isolated tube-shaped potentials oriented along the z axis is formed by two BD standing waves, and an extra RD elliptical Gaussian traveling beam is applied to weakly confined atoms in the z direction. The beam waist $w^y_{s,r}$ in the y direction is large enough that the traveling wave does not affect the BD potential shape in the range of the lattice region except by introducing an extra potential bias.

The Hamiltonian density in the lattice region can be approximately expressed as

$$h(x,y,z) = \sum_{\beta=x,y,z} -\frac{\hbar^2}{2m_a}\partial_\beta^2 + \sum_{\beta=x,y} U^\beta_{0,b}\cos^2(k_b\beta) + \sqrt{\frac{1}{3}}m_a g x + \sqrt{\frac{2}{3}}m_a g y + U_{0,r}\frac{2z^2}{\left(w^z_{s,r}\right)^2}.$$

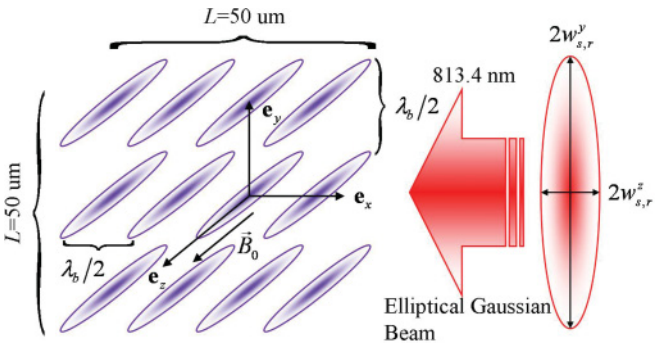

FIG. 8. (Color online) 2D BD optical lattice is formed by two standing waves along $\mathbf{e}_x$ and $\mathbf{e}_y$ with light polarization in z direction and lattice length of $L = 50\ \mu$m. The confinement on atoms in the z direction is realized by a RD z polarization traveling elliptical Gaussian wave propagating in the $\mathbf{e}_x$ direction, whose beam waists in the y and z directions are $w^y_{s,r} \gg L$ and $w^z_{s,r} = 30\ \mu$m, respectively. The quantum axis is chosen to be in the z direction, and the gravity is along the $\sqrt{1/3}\mathbf{e}_x + \sqrt{2/3}\mathbf{e}_y$ direction.

In this case, the fermionic field operator should be expanded as

$$\Psi_\alpha(\mathbf{r}) = \sum_{\vec{j},\nu_z} c_{\alpha,\vec{j},\nu_z} \Phi_{j_x}(x)\Phi_{j_y}(y)\phi_{\nu_z}(z) \quad (\alpha = e,g),$$

where $\vec{j} = (j_x, j_y)$, $\Phi_{j_x}(x)$, and $\Phi_{j_y}(y)$ are, respectively, the Wannier-Stark states in the x and y directions with indices j_x and j_y denoting the numbers of lattice sites along the corresponding directions, and $\phi_{\nu_z}(z)$ are the harmonic oscillator eigenmodes in the z direction.

Following the same process as in Sec. III, the Hamiltonian of the spin-$\frac{1}{2}$ model for fermionic atoms in a 2D lattice is given by

$$\begin{aligned} H/\hbar = &-\delta \sum_{\vec{j}} S^z_{\vec{j}} - \sum_{\vec{j}} \left(\frac{\bar{\Omega}_{\vec{j},\tilde{\nu}_z}}{2} S^+_{\vec{j}} + \text{H.c.} \right) - \sum_{\vec{j}} U_{\vec{j},\tilde{\nu}_z} \vec{S}_{\vec{j}} \cdot \vec{S}_{\vec{j}} \\ &- \sum_{\vec{j},\nu_z} \left(\frac{\delta\Omega_{\vec{j},\nu_z}}{2} S^+_{\vec{j},\nu_z} + \text{H.c.} \right) - \sum_{\vec{j},\delta\vec{j}} V_{\vec{j},\delta\vec{j},\tilde{\nu}_z} \vec{S}_{\vec{j}} \cdot \delta\vec{S}_{\vec{j},\delta\vec{j}}, \end{aligned} \tag{7}$$

where $\tilde{\nu}_z$ denotes a set of harmonic oscillators populated by atoms, two interaction strengths are defined as

$$\begin{aligned} U_{\vec{j},\tilde{\nu}_z} &= \frac{4\pi\hbar}{m_a} a^-_{eg} \left(\bar{A}^{\vec{j}}_{\tilde{\nu}_z} + 2 \sum_{\delta\vec{j}>0} \bar{A}^{\vec{j}+\delta\vec{j}}_{\tilde{\nu}_z} \right), \\ V_{\vec{j},\delta\vec{j},\tilde{\nu}_z} &= \frac{8\pi\hbar}{m_a} a^-_{eg} \bar{A}^{\vec{j}+\delta\vec{j}}_{\tilde{\nu}_z}, \end{aligned}$$

and the spin difference $\delta\vec{S}_{\vec{j},\delta\vec{j}} = \frac{1}{2}(\vec{S}_{\vec{j}+\delta\vec{j}} + \vec{S}_{\vec{j}-\delta\vec{j}}) - \vec{S}_{\vec{j}}$. Again, the primary part of intersite interactions has been effectively involved in $U_{\vec{j},\tilde{\nu}_z}$. The last two terms in Eq. (7) can be considered as perturbations. The thermally averaged two-body interaction energy is expressed as $\langle U_{\vec{j},\tilde{\nu}_z} \rangle_T = u\xi$, where the thermal-independent part is

$$\begin{aligned} u = 4\pi \sqrt{\frac{\hbar\omega_z}{m_a}} a^-_{eg} \prod_{\beta=x,y} \int |\Phi_0(\beta)|^2 \\ \times \left(|\Phi_0(\beta)|^2 + \sum_{\delta j_\beta > 0} 2|\Phi_{\delta j_\beta}(\beta)|^2 \right) d\beta. \end{aligned} \tag{8}$$

The first term in round brackets corresponds to the collisions of atoms in a single lattice site, while the second term denotes the primary part of intersite interactions.

The strength u of the two-body interactions without involving the intersite collisions [i.e., omitting the second term in the round brackets of Eq. (8)] can be in a weakly interacting regime ($u \ll \langle\Omega\rangle_T$) for a shallow optical lattice and reaches a strongly interacting regime ($u \gg \langle\Omega\rangle_T$) by enlarging the lattice potentials, as show in Fig. 9(a). However, when we take into account the effect of intersite collisions, the interaction strength u is always larger than the thermally averaged Rabi frequency $\langle\Omega\rangle_T$ [Fig. 9(b)], and hence atoms are in a strongly interacting regime.

For simplicity, we assume that $N = 3000$ atoms are trapped in the center of the lattice region with each lattice site being populated by two atoms. Figure 10(a) displays the dependence of the collision-induced frequency shift $\delta\omega_{eg}$ on the lattice potential $U^x_{0,b}$ in the x direction and the thermally averaged

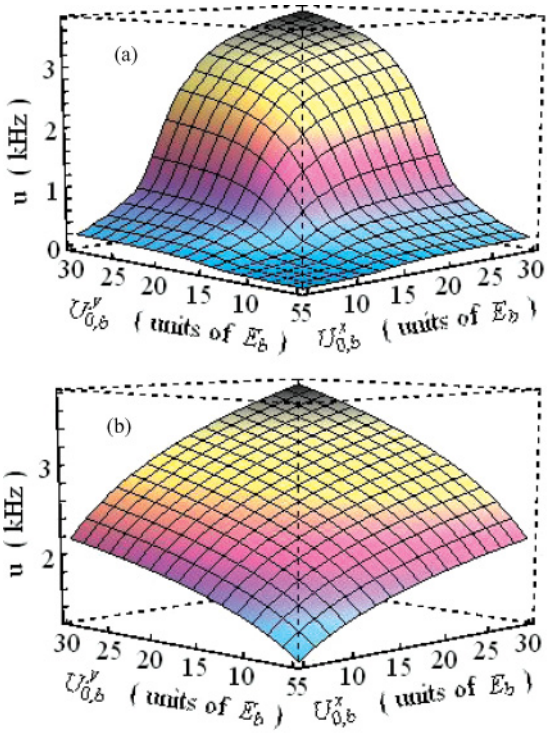

FIG. 9. (Color online) (a) Interaction energy u as functions of lattice potentials in x and y directions without involving the intersite collisions. The varying range of u covers both of the weakly and strongly interacting regimes. (b) The interaction strength u including the intersite collisions, which is only in the strongly interacting regimes. For both figures, the s-wave scattering length $|a^-_{eg}|$ is about $40a_0$ [21], the atomic temperature is $T = 3\ \mu$K, and the RD trap depth is $U_{0,r} = -37E_r(-6\ \mu\text{K})$.

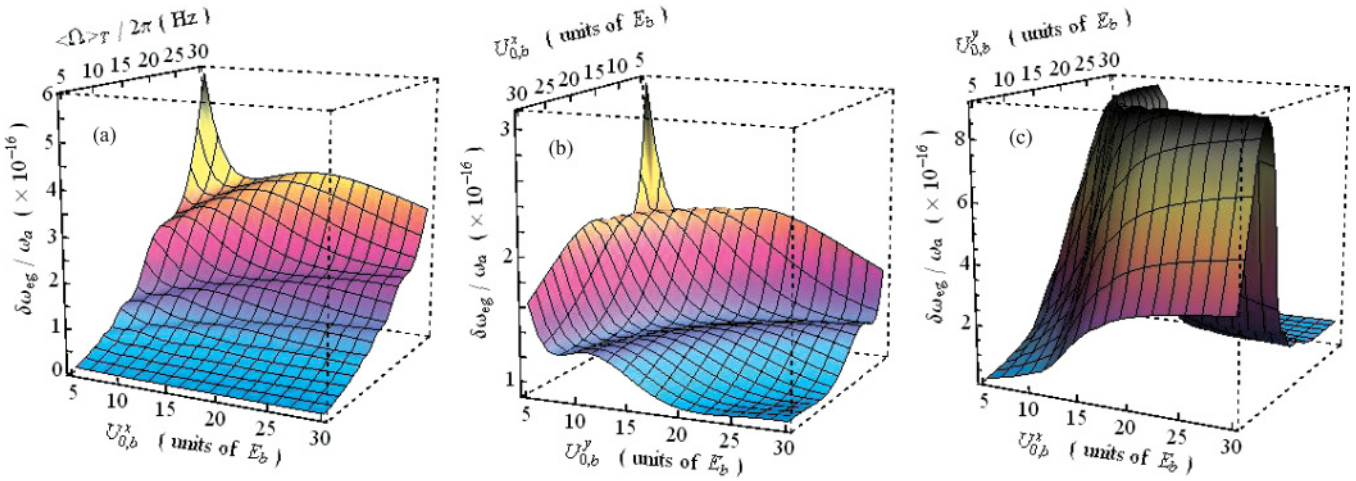

FIG. 10. (Color online) (a) Collision-induced frequency shift involving intersite collisions as functions of lattice potential in the x direction and the thermally averaged Rabi frequency $\langle\Omega\rangle_T$. The lattice potential in the y direction is fixed at $U^y_{0,b} = 30E_b$. (b) Collisional shift including intersite interactions as functions of the lattice potentials in the x and y directions with $\langle\Omega\rangle_T = 2\pi \times 22.5$ Hz. (c) Collisional shift without involving intersite interactions. The thermally averaged Rabi frequency is the same as for (b). All the other parameters are the same as for Fig. 9.

Rabi frequency $\langle\Omega\rangle_T$, from which one can obtain the features of the 2D lattice clock: (i) Increasing the interaction strength u can suppress the collisional shift $\delta\omega_{eg}$ for $u \gg \langle\Omega\rangle_T$, and (ii) $\delta\omega_{eg}$ increases with enlarging $\langle\Omega\rangle_T$ due to the larger excitation inhomogeneity. Figure 10(b) shows the collisional shift $\delta\omega_{eg}$ in a 2D optical lattice clock, which includes the intersite interactions, as functions of the lattice potentials in two directions $U^x_{0,b}$ and $U^y_{0,b}$. Since the interaction energy u always surpasses the thermally averaged Rabi frequency $\langle\Omega\rangle_T$, $\delta\omega_{eg}$ is suppressed as $U^{x,y}_{0,b}$ is increased. However, since we choose a shallow optical lattice here, the fractional collisional shift is at the 10^{-16} level.

In order to clearly demonstrate the effect of intersite collisions on the clock frequency shift, we show $\delta\omega_{eg}$ without involving the intersite collisions in Fig. 10(c) for comparison. One can see that $\delta\omega_{eg}$ strongly increases as $U^{x,y}_{0,b}$ is increased in the weakly interacting regime. However, when the strength u of two-body interactions exceeds the thermally averaged Rabi frequency $\langle\Omega\rangle_T$, $\delta\omega_{eg}$ is significantly suppressed in the strongly interacting regime because the singlet and triplet states are well separated. Therefore, the intersite collisions strongly affect the clock-transition frequency in the weakly interacting regime, while the collisions of atoms at a single lattice site mainly contribute to the collisional shift in the strongly interacting regime.

V. SUMMARY

In a BD lattice, atoms are trapped in the intensity minima of a lattice field, which strongly reduces the higher-order light shift and makes the BD lattice clock an attractive candidate to realize a high-performance optical clock. In this paper, we have investigated the collisional shift in a shallow BD optical lattice, where the intersite interactions of atoms in different lattice sites can no longer be neglected. Since the BD magic wavelength λ_b is less than half of the RD one λ_r, a relatively much larger lattice potential is required to tightly confine atoms in each lattice site.

For a 1D optical lattice, since atoms can be only tightly confined in one direction while the atomic dynamics should be thermally averaged in the other two directions, the energy separation between the singlet and triplet states is much smaller than the thermally averaged Rabi frequency (i.e., the weakly two-body interacting regime). In this case, the collision-induced frequency shift monotonically increases as the strength of the two-body interactions is increased (i.e., a larger lattice potential leads to a larger collisional shift). One may expect to decrease the lattice potential in order to reduce the interaction energy of atoms in a single lattice site. However, the intersite collisions strongly increase and mainly affect the clock-transition frequency for a shallow optical lattice, for which the collisional shift cannot be strongly reduced and a relatively larger Doppler shift will be introduced to an optical lattice clock.

For a 2D optical lattice, atoms can be tightly confined in two directions, which makes the collision strength of atoms at a single lattice site cover both the weakly and strongly interacting regimes. In the strongly interacting regime, since the singlet and triplet states are well separated in energy, the collisional shift can be dramatically suppressed by increasing the atomic interaction energy. One may expect that, if the lattice potentials are reduced from the strongly interacting regime to the weakly interacting regime, the collisional shift would first strongly increase and then significantly decrease when the strength of atomic interaction is smaller than the thermally averaged Rabi frequency. However, due to the large intersite collisions in a shallow optical lattice, the two-body interaction strength is always larger than the thermally averaged Rabi frequency. Hence, the collisional shift monotonically increases with the lattice potentials being reduced.

For both 1D and 2D lattice clocks, the fractional collisional shifts are at the 10^{-16} level for an effective misalignment angle $\Delta\theta \sim 10$ mrad of the probe beam. Suppressing fermion collision shifts requires the homogeneous excitation, the exact control of the Rabi pulse area, and the reasonably

homogeneous atomic distribution. Additionally, a 3D BD optical lattice is still an interesting and challenging choice, where a high number of quantum absorbers is maintained but lattice traps well separate each atom.

ACKNOWLEDGMENTS

The author would like to thank Hidetoshi Katori for useful discussions and suggestions. This work was supported by the Japan Society for the Promotion of Science (ID No. P09229).

[1] M. Takamoto, F. L. Hong, R. Higashi, and H. Katori, Nature (London) **435**, 321 (2005).
[2] F. L. Hong and H. Katori, Jpn. J. Appl. Phys. **49**, 080001 (2010).
[3] A. Derevianko and H. Katori, Rev. Mod. Phys. **83**, 331 (2011).
[4] H. Katori, Nature Photonics **5**, 203 (2011).
[5] K. Numata, A. Kemery, and J. Camp, Phys. Rev. Lett. **93**, 250602 (2004).
[6] M. Notcutt, L. S. Ma, A. D. Ludlow, S. M. Foreman, J. Ye, and J. L. Hall, Phys. Rev. A **73**, 031804(R) (2006).
[7] S. A. Webster, M. Oxborrow, S. Pugla, J. Millo, and P. Gill, Phys. Rev. A **77**, 033847 (2008).
[8] J. Alnis, A. Matveev, N. Kolachevsky, Th. Udem, and T. W. Hänsch, Phys. Rev. A **77**, 053809 (2008).
[9] G. Santarelli, C. Audoin, A. Makdissi, P. Laurent, G. J. Dick, and A. Clairon, IEEE Trans. Ultrason. Ferroelectr. Freq. Control **45**, 887 (1998).
[10] J. Lodewyck, P. G. Westergaard, A. Lecallier, L. Lorini, and P. Lemonde, New J. Phys. **12**, 065026 (2010).
[11] G. K. Campbell *et al*., Science. **324**, 360 (2009).
[12] Y. B. Band and A. Vardi, Phys. Rev. A **74**, 033807 (2006).
[13] Y. B. Band and I. Osherov, Phys. Rev. A **84**, 013822 (2011).
[14] H. Katori, M. Takamoto, V. G. Pal'chikov, and V. D. Ovsiannikov, Phys. Rev. Lett. **91**, 173005 (2003).
[15] V. D. Ovsiannikov, V. G. Pal'chikov, H. Katori, and M. Takamoto, Quantum Electron. **36**, 3 (2006).
[16] P. Rosenbusch, S. Ghezali, V. A. Dzuba, V. V. Flambaum, K. Beloy, and A. Derevianko, Phys. Rev. A **79**, 013404 (2009).
[17] H. Katori, K. Hashiguchi, E. Yu. Il'inova, and V. D. Ovsiannikov, Phys. Rev. Lett. **103**, 153004 (2009).
[18] Y. Y. Jiang *et al*., Nature Photonics **5**, 158 (2011).
[19] M. Takamoto, T. Takano, and H. Katori, Nature Photonics **5**, 288 (2011).
[20] K. Gibble, Phys. Rev. Lett. **103**, 113202 (2009).
[21] M. D. Swallows *et al*., Science **331**, 1043 (2011).
[22] T. Akatsuka, M. Takamoto, and H. Katori, Nature Physics **4**, 954 (2008).
[23] Ch. Lisdat, J. S. R. Vellore Winfred, T. Middelmann, F. Riehle, and U. Sterr, Phys. Rev. Lett. **103**, 090801 (2009).
[24] M. Bishof, M. J. Martin, M. D. Swallows, C. Benko, Y. Lin, G. Quéméner, A. M. Rey, and J. Ye, Phys. Rev. A **84**, 052716 (2011).
[25] A. D. Ludlow, N. D. Lemke, J. A. Sherman, C. W. Oates, G. Quéméner, J. von Stecher, and A. M. Rey, Phys. Rev. A **84**, 052724 (2011).
[26] M. Takamoto, H. Katori, S. I. Marmo, V. D. Ovsiannikov, and V. G. Pal'chikov, Phys. Rev. Lett. **102**, 063002 (2009).
[27] A. V. Taichenachev, V. I. Yudin, V. D. Ovsiannikov, V. G. Pal'chikov, and C. W. Oates, Phys. Rev. Lett. **101**, 193601 (2008).
[28] P. Lemonde and P. Wolf, Phys. Rev. A **72**, 033409 (2005).
[29] A. M. Rey, A. V. Gorshkov, and C. Rubbo, Phys. Rev. Lett. **103**, 260402 (2009).
[30] A. V. Gorshkov *et al*., Nature Physics **6**, 289 (2010).
[31] S. Blatt, J. W. Thomsen, G. K. Campbell, A. D. Ludlow, M. D. Swallows, M. J. Martin, M. M. Boyd, and J. Ye, Phys. Rev. A **80**, 052703 (2009).
[32] M. Bishof, Y. Lin, M. D. Swallows, A. V. Gorshkov, J. Ye, and A. M. Rey, Phys. Rev. Lett. **106**, 250801 (2011).